A new experimental setup for the simulation of surface crack formation in the continuous casting process

Roman Krobath[1], Christian Bernhard[2]

[1]Montanuniversitaet Leoben
Franz-Josef-Strasse 18, 8700 Leoben, Austria
Phone: +43 3842 402-2254
Email: roman.krobath@unileoben.ac.at

[2] Montanuniversitaet Leoben
Franz-Josef-Strasse 18, 8700 Leoben, Austria
Phone: +43 3842 402-2220
Email: christian.bernhard@unileoben.ac.at

Keywords: continuous casting, surface cracks, transverse cracking, microalloyed steel

INTRODUCTION

Surface cracks on semifinished continuously cast products remain a widespread problem in the steel industry. Without post-processing steps, these defects can lead to massive quality problems in the finished sheets. The formation of transverse cracks is directly related to the ductility of the strand shell, and therefore on the material properties during the casting process and the mechanical and thermal stresses developed in secondary cooling and bending/unbending. In particularly, during unbending, embrittlement can become high when the temperature of the strand surface reaches the second ductility trough. The frequency of surface cracks is increased when pre-defects in the strand shell, such as oscillation marks and abnormally large austenite grains, are present [1-5]. Many studies have investigated the hot ductility of steels via tensile tests. Laboratory experiments determine the reduction of area (RA) of the ruptured tensile samples, which relates to the ductility, as functions of the testing temperature (T), under the influence of composition, strain rate, heating/cooling conditions, and other factors; these studies are summarized e.g. in Schwerdtfeger [6] and Mintz [3]. Tensile tests are useful instruments for determining material behaviors at higher temperatures and they supply valuable information regarding the temperatures that should be avoided during deformation of the strand surface, but there exist some limitations for directly relating laboratory RA–T curves to the prediction of surface cracks in the continuous-casting machine:

- The stress/strain state differs between hot tensile testing and continuous casting: Cracking on the strand surface normally occurs when the material accumulates a critical strain (up to ~2%). The first difference is the constriction of the material in the tensile test before rupture. Next, compared to the continuous casting process, the longitudinal strain prior to rupture at cracking remains high for low RA – values [2, 7, 8]. These values, however, indicate cracking susceptibility of the surface in continuous casting, although they are much higher than those in the strand shell.
- These differences in the stress/strain state accompany other material phenomena in the tensile tests: At higher temperatures, dynamic recrystallization, which recovers ductility by boundary migration, can occur. The incidence of dynamic recrystallization increases at increased strain rates and higher elongations ($e > \sim 10\%$) [3, 9]. According to these values, it would be difficult for dynamic recrystallization to occur on the strand surface.
- Particularly the second ductility trough, determined by hot tensile testing, consists of two embrittlement factors. At higher temperatures, precipitates along austenite grain boundaries cause the decrease in ductility. Microalloyed steels in particular show this effect. At lower temperatures, the austenite-to-ferrite transformation causes embrittlement. The underlying mechanism should be the concentration of strains at thin ferrite films along the austenite grain boundaries, which begin to form at the A_{R3} temperature during the γ-to-α transformation [2]. Inducing strain in the material can generally increase the A_{R3} temperature of steels. This phenomenon is called deformation-induced ferrite. The starting temperature for the formation of this ferrite is strongly influenced by the total strain, strain rate, and grain size. Higher strains and lower strain rates correlate to earlier ferrite formation. For coarser austenite grains, the critical strain triggering the formation is even higher. Studies show that deformation-induced ferrite can form at strains up to 2% [9-11]. Because of the high strains in tensile test, the formation of deformation-induced ferrite can distort the second ductility trough used to predict surface crack formation during continuous casting.
- Scale formation on the strand surface in the secondary cooling zone, which could influence the surface crack formation, does not occur in tensile testing. Tensile tests are performed in inert atmospheres with no formation of scale in the laboratory.

- The solidification structure with directly grown dendrites and columnar austenite grain structures is significant for the strand surface. As the hot tensile test specimens are reheated, a new austenite grain structure forms that differs from the coarsened and columnar austenite grain structure. This topic is discussed in the next chapter.

Based on this knowledge, a new experimental setup for the prediction of surface crack formation in continuous casting was invented in Comet-K2 and K1-MET projects at the Institute of Ferrous Metallurgy at Montanuniversitaet Leoben. The experimental setup and a test series for the influence of the Nb content on the surface cracking susceptibility is described in this paper.

EXPERIMENTAL SETUP

The In-Situ Material Characterization–Bending (IMC-B) test can be used to predict the susceptibility of surface crack formation under continuous casting conditions. Therefore, the test combines thermal and mechanical stresses and their effects on the surface quality of a solidified steel sample. The test can be divided into three steps, which are summarized in **Figure 1**.

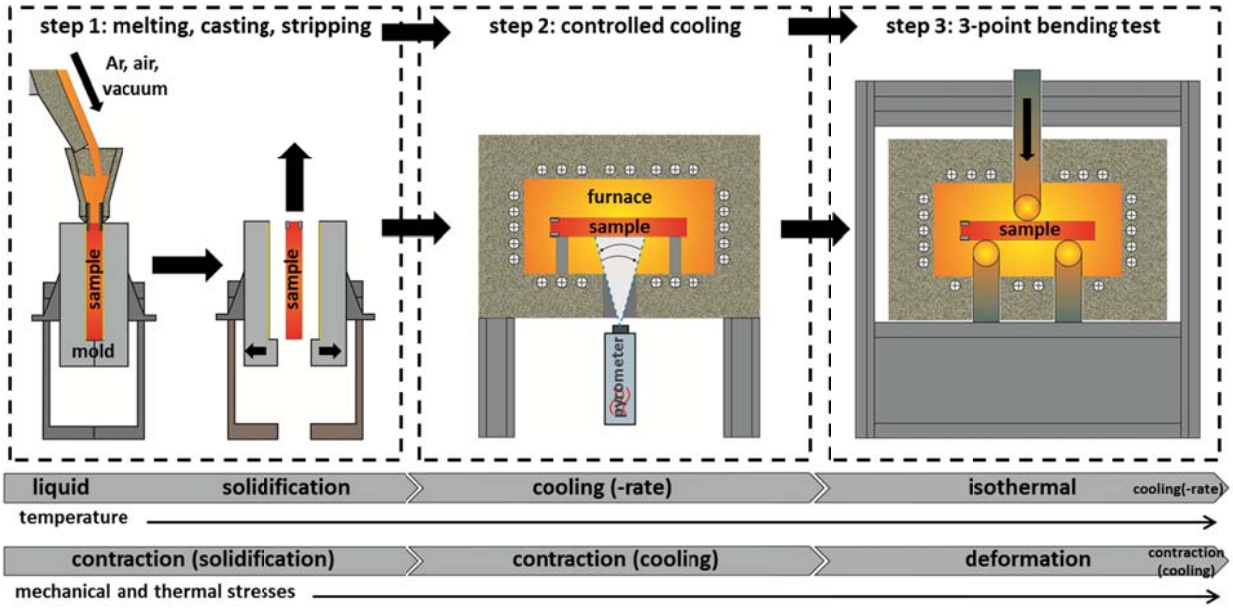

Figure 1: Principle of the IMC–B test

Step 1: Melting and solidification

The steel is melted in an induction furnace. The atmosphere can be air, inert gas (Ar, N_2), or vacuum. With these possibilities, the composition of the sample can be freely determined by adding pure alloying elements until the final steel grade is reached. For the casting process and the solidification behavior, the use of an exact casting temperature is essential. **Figure 2** shows schematically the solidification and the heat flux through the mold wall. The solidification structure of the sample is presented in figure 2a). The heat flux direction promotes directional dendrite growth. This is related to the strand shell solidification; as the structure coarsens with increasing distance from the surface, solidification phenomena such as segregation and micropore formation occur [12, 13].

The influence of the austenite grain size on the hot ductility of steels is well known. Coarse austenite grains broaden the temperature range of the ductility trough and ensure lower ductility [14, 15, 16]. Figure 2b) shows the columnar austenite grain structure in the sample (side view). On the surface of the sample, the grain structure is finer, with increasing coarseness farther from the sample surface. This coarsening effect also occurs in steel slabs; it is reduced to the thermal history and the residual time at higher temperatures of the material with increasing distance from the slab surface [17]. The columnar grain structure typically causes deterioration in the hot ductility. Once a crack forms, it can propagate easily along the grain boundaries [18].

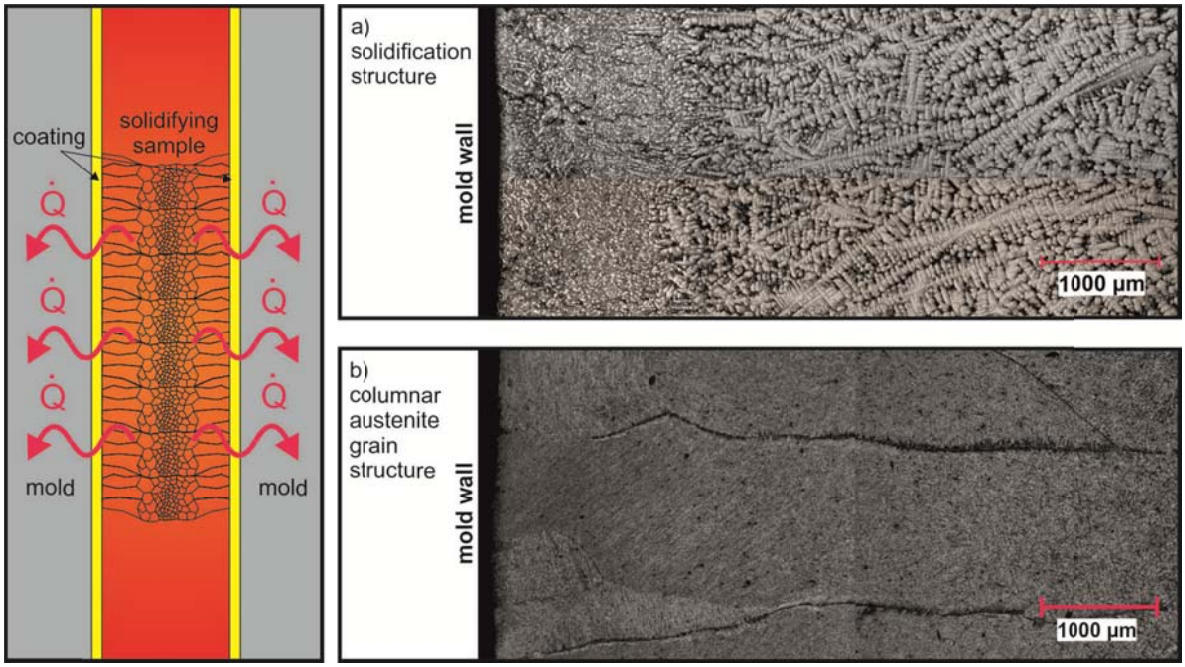

Figure 2: left: schematic view of the solidifying sample; a) solidification structure visualized with Bechet and Beaujard etching; b) columnar austenite grain structure after 3% Nital etching

The sample compositions of the test series described within this work are listed in **Table 1**. All are Al-deoxidized construction steels with 0.17 wt.% C. The three steels differ in Nb content. The comparison shows the influence of the amount of microalloyed Nb on the propagation of surface cracks.

Table 1: steel compositions for present study

	C [wt.%]	Si [wt.%]	Mn [wt.%]	P [wt.%]	S [wt.%]	Al [wt.%]	Nb [wt.%]	N [ppm]
Steel 0Nb	0.17	0.4	1.55	0.01	<0.004	0.03	**0.002**	50
Steel 0.02Nb	0.17	0.4	1.55	0.01	<0.004	0.03	**0.02**	50
Steel 0.04Nb	0.17	0.4	1.55	0.01	<0.004	0.03	**0.04**	50

Step 2: Sample cooling

After stripping from the mold, the sample is cooled according to a given cooling curve. The atmosphere is not inert, so scale formation occurs. This is an additional point reflecting the more realistic conditions during the test process. The temporal sequence for the test series is shown in **Figure 3**. During cooling, the sample surface is continuously measured with the pyrometer.

At a time of 45 s, the mold is stripped; subsequently, the surface temperature is controlled. The sample cools to 1050°C, where a temperature-homogenization step is performed until the total elapsed time of 160 s. Here, we note the importance in using equal total times and temperatures for each experiment. Until this point, the temporal sequence is the same; therefore, differences in the formation of precipitations depend only on the chemical compositions of the samples. This also applies for the austenite grain structure.

The cooling is continued at various cooling rates to investigate the effects of the different cooling curves and the deformation temperature regarding the formation of surface cracks. The precipitation state of the samples varies with the steel composition and the target temperature. At 580 s, the sample surface reaches the bending temperature. It follows an additional temperature homogenization step until a total time of 700 s. These cooling curves are related to a calculated cooling strategy for a slab caster with a thickness of 225 mm and a casting speed of 1.2 m/min [19]. After the bending process, the samples are smoothly cooled to room temperature in a furnace to minimize thermally induced and transformation-induced stresses and strains on the surface, which can affect the crack propagation after deformation. For a good visualization of the prior austenite grain boundaries at room temperature after etching, some samples were quenched after the deformation process. This is explained in the results chapter in greater detail.

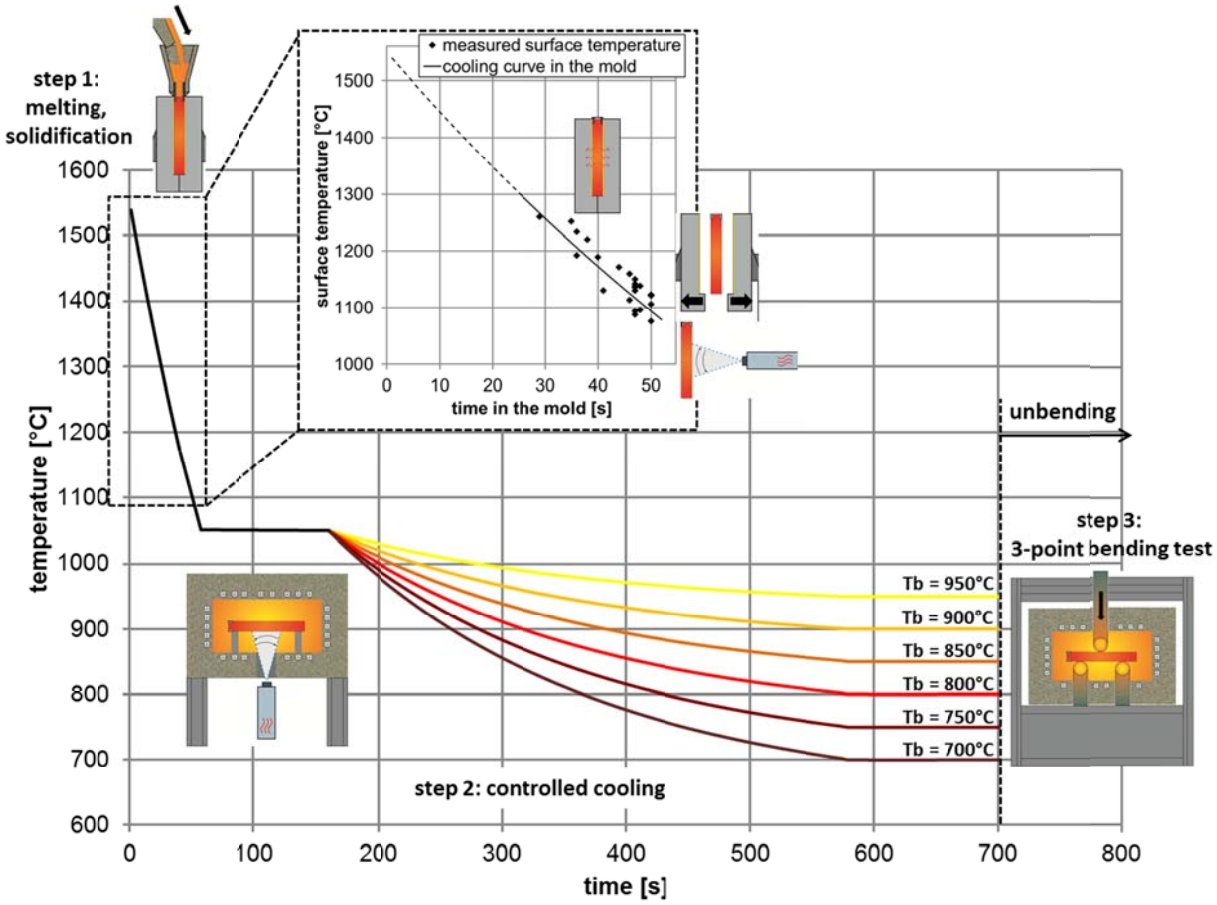

Figure 3: Upper diagram depicts measured surface temperature after different holding times in the mold. Temperature sequence for the test series, with schematics of samples at each step

Step 3: Isothermal three-point bending test

At 700 s, the strand reaches the unbending, or straightening, zone. To simulate accumulated strains during the straightening phase, an isothermal three-point-bending test with a constant stamp velocity is performed. To determine the influence of the deformation temperature and therefore the strand surface temperature on the formation of surface cracks during unbending, the test is performed at temperatures between 700°C and 950°C at 50°C intervals. The test is simulated with a three-dimensional model using the finite element method (FEM) software Abaqus. **Figure 4** shows the calculated strain state in the *x*-direction for the present test series. The stamp moves against the *z*-direction at a constant velocity and deforms the sample on the lower surface (upper strand surface in the continuous casting machine during unbending). The strain rate is $6 \cdot 10^{-4} s^{-1}$ and the maximum induced strain in the *x*-direction is ~1.5%. During the bending test, the load is recorded with a data-acquisition unit.

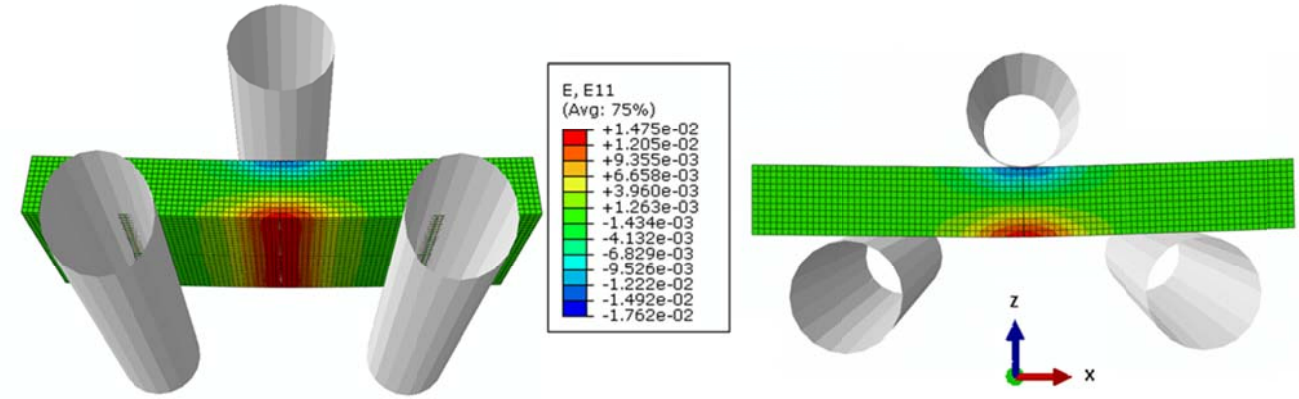

Figure 4: Abaqus simulation of the bending test; left: 3-D bottom view; right: side view; middle: strain values at the end of the load-step

Figure 5 provides all physical dimensions of the tested samples, with thicknesses of 23 mm, widths of 58 mm, and lengths of 180 mm. As explained before, the samples are slowly cooled to room temperature after deformation. After cooling, the surface is cleaned and descaled. Next, the elongated sample surface is investigated within 40 mm to the left and right of the bending axis (**Figure 5**, right). This represents the strain-influenced area, determined with the Abaqus simulation. Investigation is implemented with a stereomicroscope, which enables the detection of defects with a minimum size of 50 µm. The encountered defects are registered for detailed investigation with light microscopy and scanning electron microscopy (SEM).

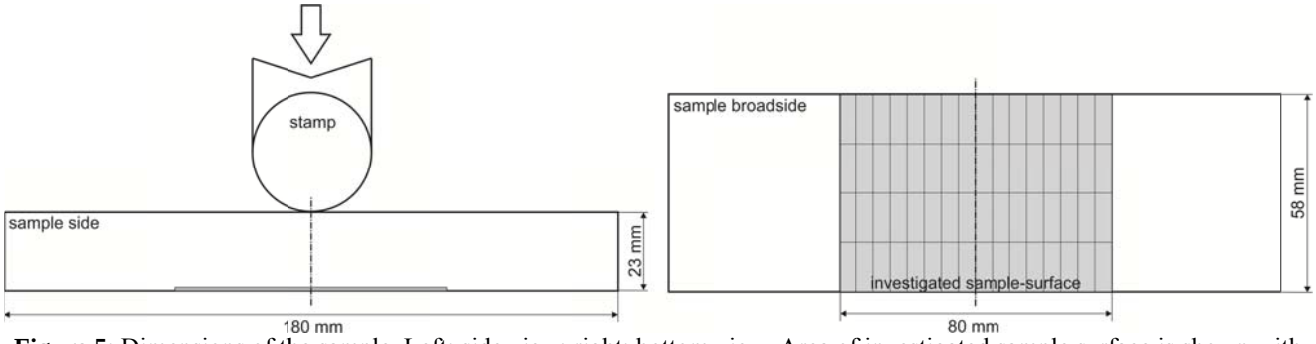

Figure 5: Dimensions of the sample. Left: side view; right: bottom view. Area of investigated sample surface is shown with examination pattern

RESULTS

Crack population

Every experiment was performed twice for each temperature. **Figure 6** presents the results for the crack investigations with the stereomicroscope. The upper line of each graph indicates zero cracks on the sample surface. From the top down, the number of cracks increases. The ordinate shows the bending temperature. Notably, after bending, the samples are cooled slowly to minimize the thermal and transformation-induced stresses. In the leftmost diagram (6a) the determined results for steel with 0.002 wt.% Nb are seen. At the high bending temperature of 950°C, and again in the lower region at 700 and 750°C, no cracks are initiated on the samples' surfaces. At 800 and 900°C, sample 1 shows no cracks; in sample 2 one crack formed. 850°C is shown as the worst deforming temperature for this steel grade, with one crack in each sample.

The results for an addition of 0.02 wt.% Nb are presented in 6b). The high-temperature range of 950 and 900°C shows the best behavior. At 950°C, one crack formed in sample 2. Obviously critical are the tests at 850°C (four cracks in sample 1, seven in sample 2) and 800°C (four cracks each). The surface ductility improves at 750°C (two cracks each) and 700°C (one crack in sample 2, two in sample 1). A further increase in the Nb content to 0.04 wt.% induces bad surface ductility at all bending temperatures. The trough is moved from 850°C (6b) to 950°C, with higher crack numbers (seven and nine surface cracks). The behavior improves slightly for bending temperatures of 900°C to 700°C, but every sample features between three and six cracks. The ductility decreases again at 750°C and 700°C.

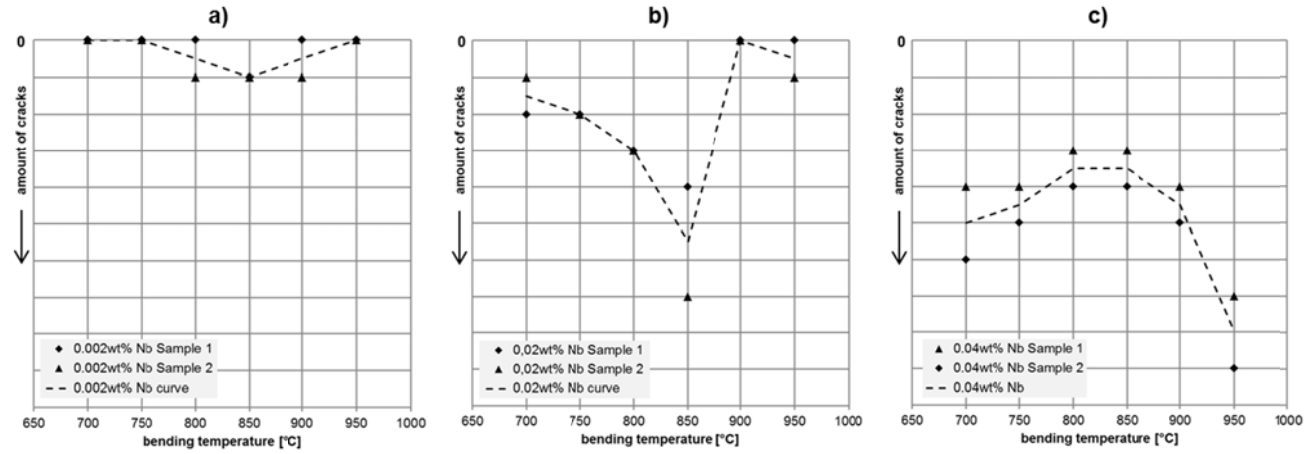

Figure 6: Number of cracks with respect to steel composition and deformation temperature; each temperature is tested twice (samples 1 and 2); curves represent the mean values. (a) Steel 0Nb, (b) steel 0.02Nb, and (c) steel 0.04Nb

Crack morphology

The sample surface was investigated with the stereomicroscope using a pattern (**Figure 5**, right side). Every crack was scanned and recorded. Examples of documented cracks are shown in **Figure 7**. The lengths range from 450 to 1200 µm. The minimum detected crack length is ~200 µm. The pictures a) and b) show cracks at the broad side. In picture c), a crack propagated from the sample edge is imaged. The percentage of edge cracks is 24%.

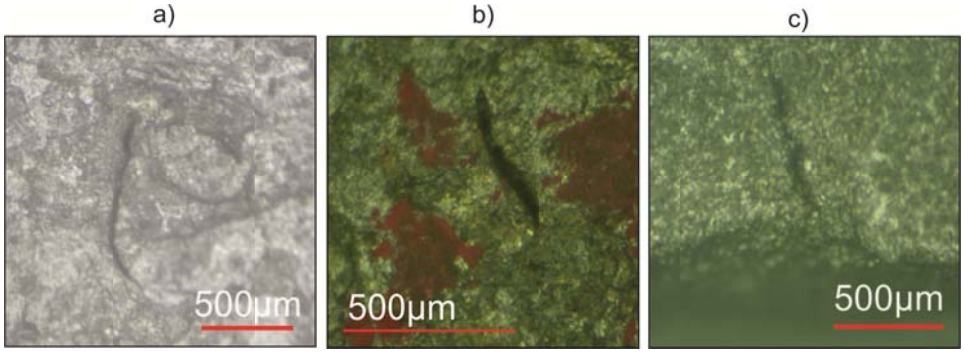

Figure 7: Examples of formed cracks observed with the stereomicroscope. a) and b) Cracks on the sample broadside; c) crack at the sample edge

Selected cracks were investigated with SEM. **Figure 8** shows examples of the examinations. In picture a), a crack at the surface in the prior austenite grain boundaries can be seen. It is ~500 µm long and ends at a triple point in the lower part of the picture. In picture b), a crack area is given; the crack and the surrounding matrix were deep-frozen with liquid N. This separated piece was broken with selective force application. After rupture, the whole area of the high-temperature crack can be investigated. The length and depth are clearly apparent, but significant characteristics like prior austenite grain boundaries also become visible. The crack in the example is ~400 µm long and ~150 µm deep. In the crack area, prior austenite grain boundaries are visible. The brittle zone, caused by the deep-frozen rupture, can be easily distinguished from the high-temperature crack area. The surface line is also marked: a significant roughness caused by the casting, solidification process, and scale formation is visible. Picture c) shows a special detail of an austenite grain boundary on a crack area. It is a coincidence of three austenite grains, called a triple point.

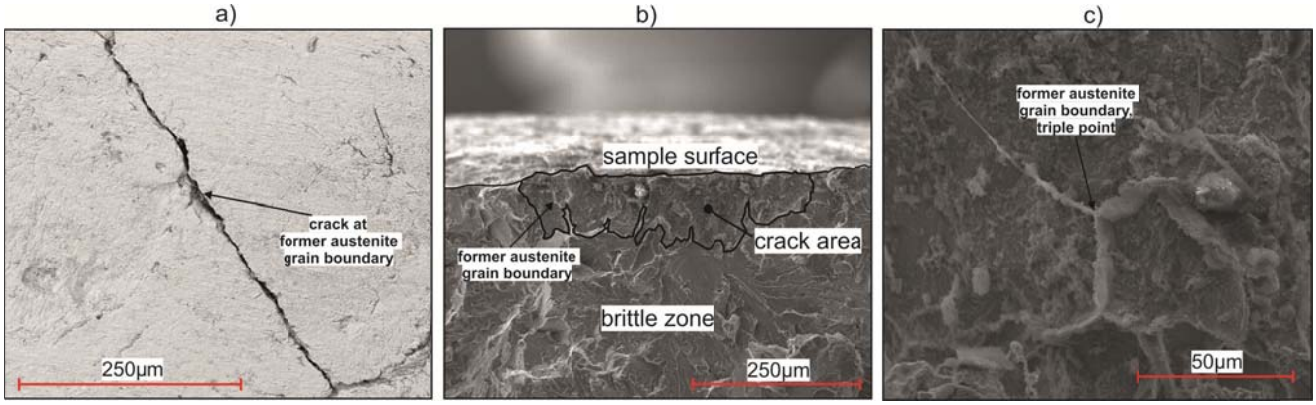

Figure 8: Cracks investigated with SEM. a) crack on the descaled sample surface; b) ruptured sample with the crack formed in the bending experiment and the brittle zone; c) detail of a crack area and triple point

Austenite grain growth

As mentioned before, the austenite grain size has a significant influence on the hot ductility of RA–T tests. The RA values decrease for increasing grain sizes. The ductility trough broadens to include higher and lower temperatures [14, 20]. The IMC-B test allows the observation and identification of austenite grain growth depending on the cooling strategy and composition. In the present test series, in addition to the crack investigations, the influence of the Nb content on the austenite grain growth during cooling was examined. Therefore, selected samples were quenched after deformation, to increase the visibility of prior austenite grain boundaries at room temperature. The cooling sequence for the examinations is shown in **Figure 9** on the left-hand side. The samples were deformed at 700°C and afterwards quenched. To allow surface polishing, the casting surface was ground to a depth of 0.5 mm. After polishing, the samples were etched with a 3% Nital solution (3% HNO_3). In **Figure 9** on the right side, an etched microsection of steel with 0.002 wt.% Nb is shown. The austenite grains with

different crystallographic orientations and grain boundaries are clearly visible. These are the best conditions for measuring the austenite grain size.

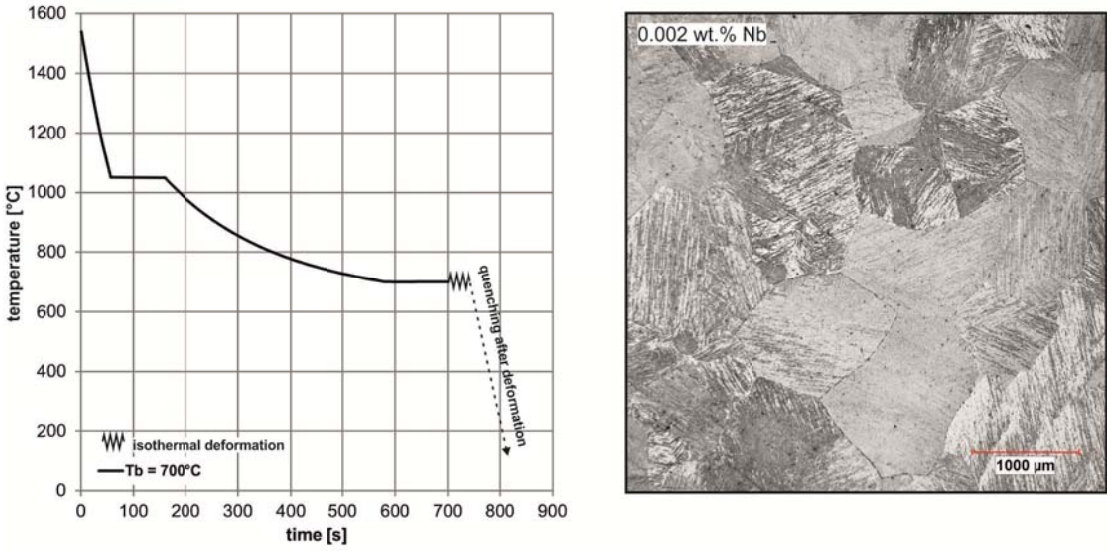

Figure 9: left side: thermal sequence for the austenite grain investigations; right side: ground and etched sample surface example: steel with 0.002 wt.% Nb

The analysis was done by the intercept method. The intercept length was measured and converted to the equal-circle diameter (ECD) [21, 22]. **Figure 10** presents, on the left hand, the distributions for the steels with different Nb contents. A histogram is displayed for steel with 0.04 wt.% Nb. The progression of the curves is very similar. The peak height is related to the total number of counted grain intercepts. On the right hand, the mean ECD with respect to the steel composition, and therefore the amount of Nb, is given. The mean ECD for steel 0Nb is 907 µm. The addition of Nb causes a continuous decrease in grain sizes. This is as expected and is discussed in the next chapter.

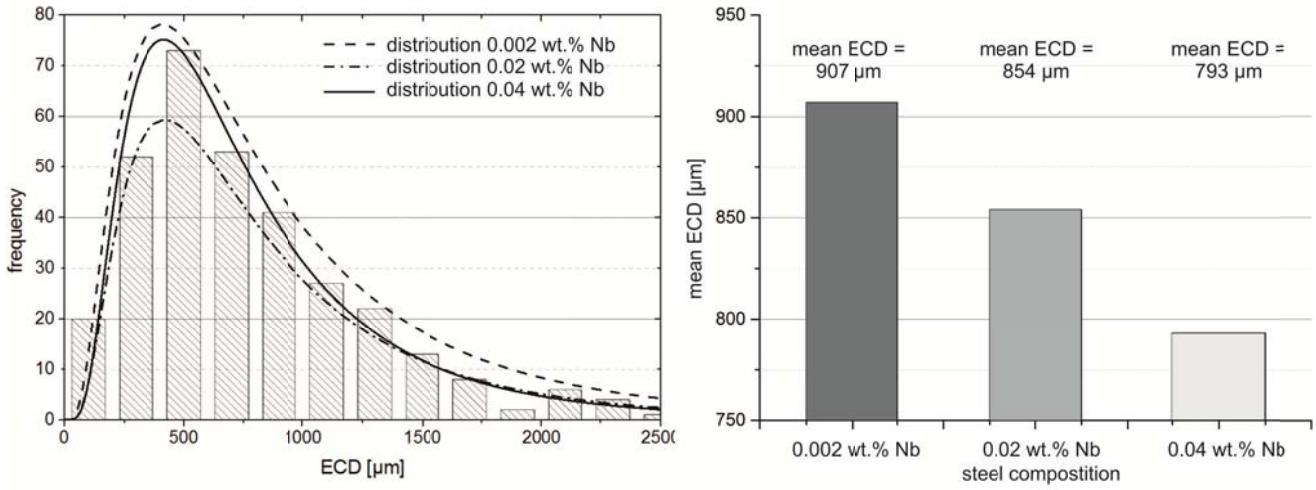

Figure 10: left side: ECD distributions for the different Nb contents; right side: mean ECD for 0.002 wt.% to 0.04 wt.% Nb

DISCUSSION

The formation of cracks on the surfaces of the cast samples is strongly influenced by the Nb content and the bending temperature. Existing literature ascribes the embrittlement of Nb-microalloyed steels to the formation of Nb(C,N), which are located at the austenite grain boundaries. The ductility trough is significantly deepened and broadened especially to higher temperatures. The effect becomes more intense as the Nb content is increased (from 0.017 to 0.074 wt.% Nb) [23]. In the

present test series, the sample was only deformed to a maximum strain of 1.5%, based on the deformations during unbending. This means that no dynamic recrystallization and significantly less deformation-induced precipitates should exist compared to specimens subjected to hot tensile tests. Therefore, the increased ductility caused by dynamic recrystallization at higher temperatures is prevented. In the experiment, the steel with 0.04 wt.% Nb shows the worst behavior at the highest bending temperature of 950°C. In **Figure 11**, the experiments are plotted in different categories depending on the deformation temperature and the actual Nb content:

- class 1: no surface cracks—risk for surface cracking under the tested temporal sequence is very low.
- class 2: 0 < number of surface cracks ≤ 2—first ductility losses occur at the surface; the temperatures could be critical during unbending (right side shows lower crack distribution).
- class 3: >2 surface cracks—more than two defects on the sample, clearly reduced ductility, temperatures should be prevented during unbending (right side: upper crack distribution).

The dotted line represents the critical range for surface cracking following the described classes. It demonstrates that a critical Nb content exists for the tested conditions. The remedy could be an even slower cooling sequence to deformation temperatures of 1000°C and higher. As the Nb content decreases, the higher deformation temperatures of 900 and 950°C become safe again. The temperatures of 800 to 850°C should be prevented. Without Nb, the first defects form at temperatures of 800 to 900°C. The formation of fine AlN precipitates could decrease the ductility.
The occurrence of precipitates becomes visible in the observation of the austenite grain size. Precipitates can cause the pinning of grain boundaries, which would prevent grain growth in a certain direction [24]. The smaller grain size at higher Nb content indicates the presence of Nb(C,N) at the grain boundaries.

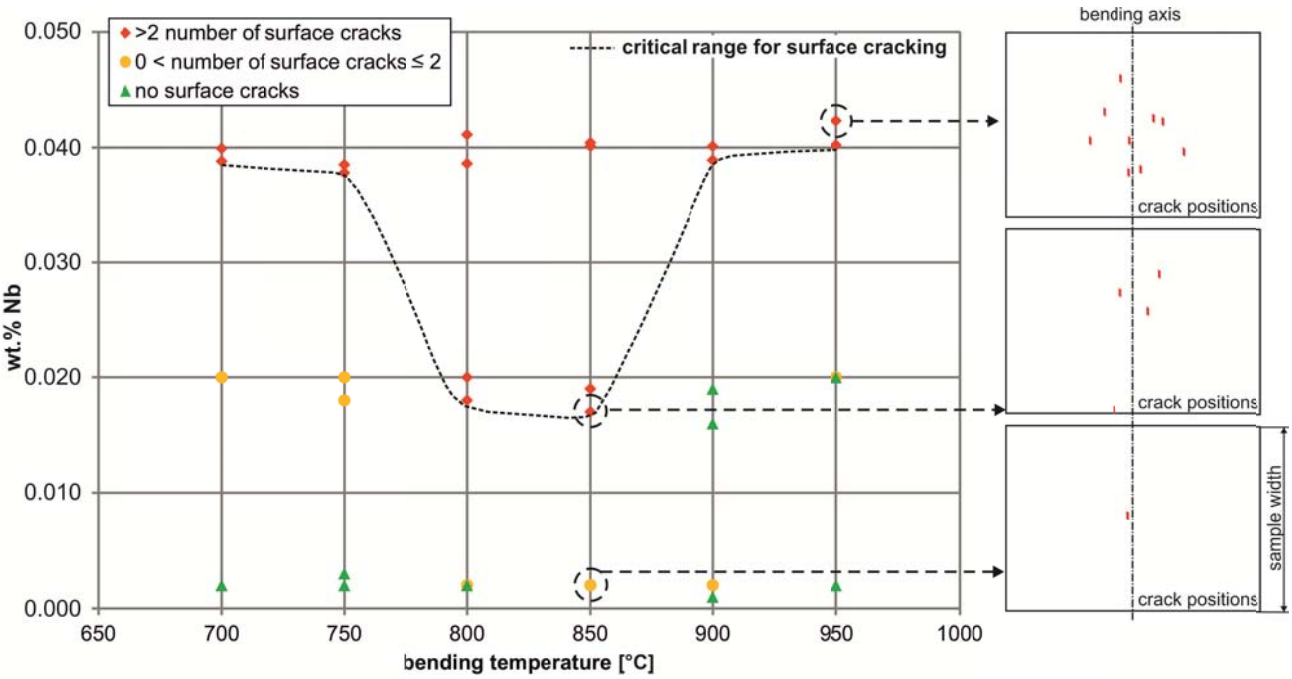

Figure 11: critical range for surface cracking, depending on the present Nb content and the deformation temperature (left side); crack distributions on the sample surface (right side)

At the lower bending temperatures of 750 and 700°C, steel 0Nb shows no loss in ductility. This should be the range of the austenite-to-ferrite transition and the associated ductility trough. Tests performed with a maximum strain of 6.5% also revealed no surface cracks at these temperatures. This inspired the investigation of the steels using a high-temperature laser scanning confocal microscope (HT-LSCM), which is an efficient tool to observe the transformation of γ to α and the transition temperature for the phases that appear first [24]. The sample is heated to a holding temperature of 1320°C. After a holding time of 10 min, the sample is cooled according to the thermal cycle for the bending temperature of 700°C (**Figure 3**). The thermal etching effect results in the optical appearance of the grain boundaries after a certain time. Austenite grains

become visible, in addition to phase transformations during the subsequent cooling. The first transformations appeared between 724 and 728°C for the three steels. Note that HT-LSCM recognizes the early changes in the structures. According to these investigations, small amounts of ferrite were present in all three steels at the bending temperature of 700°C. Looking at **Figure 6**, only the steel with 0.04 wt.% Nb shows decreased ductility at this temperature. At 0.02 wt.% Nb, the ductility is improved; for the steel without Nb, no cracks form on the sample surface. This could be related to the first phases that appeared in HT-LSCM observation. Aside from a small amount of ferrite films at the grain boundaries, the majority phase was Widmanstaetten-ferrite. This phase is obviously less harmful for the surface ductility in the performed tests.

CONCLUSION

The new testing method for the determination of the susceptibility to surface cracking under continuous casting conditions fulfills the requirements for a realistic simulation of crack formation. The characteristics are as follows:

- The adjustment of the steel composition in the induction furnace, casting of a sample with controlled casting temperature and solidification conditions, and control of the heat withdrawal (grain growth) by use of mold coatings creates a columnar grain structure with typical solidification phenomena, such as segregations and micropores.
- Setting of the sample temperature to the simulated casting process and cooling strategy (control of microstructure formation and precipitation kinetics) and the free adjustment of the temporal sequence permits the simulation of the formation of all types of surface cracks.
- The performance of an isothermal three-point bending test with a defined maximum strain and strain rate allows the adjustment of temperature, strain rate, and strain to mimic process conditions.
- Strain is limited to a few percent. This prevents dynamic recrystallization and suppresses the formation of deformation-induced precipitates and deformation-induced ferrite.

A test series with medium-carbon steel differing only in the Nb contents was performed. Cooling conditions were adjusted to mimic a slab caster with a casting speed of 1.2 m/min. The deformation in the experiment began when the strand reached the unbending stage. The investigated temperature range was 700 to 900°C with six steps. The maximum strain was 1.5%, according to the unbending step of the caster. Every experiment was done twice to demonstrate significance and reproducibility.

The results showed a clear correspondence of the formation of surface cracks to the Nb content. Without Nb, cracks only appeared around 850°C. When 0.02 wt.% Nb was added, the ductility deteriorated. A trough, again around 850°C, was observed; the higher-temperature regions were safe. At lower temperatures (700 and 750°C), cracks formed, but the ductility improved again. An addition of 0.04 wt.% Nb caused cracks in every sample. The highest crack ratio appeared at 950°C. Defining more than two cracks on the sample as critical, the range for surface cracking depending on the Nb content is as follows:

- The 0.17 wt.% C steel without Nb addition showed no critical behavior in the investigated temperature region.
- Deformation temperatures of 800 and 850°C should be prevented during deformation when 0.02 wt.% Nb is added.
- When 0.04 wt.% Nb is alloyed, the whole temperature range from 950 to 700°C is critical.

The increased susceptibility to cracking was ascribed to the higher concentration of Nb(C,N) at the austenite grain boundaries and the prevention of dynamic recrystallization at higher temperatures.

In summary, the proposed experimental method for the simulation of surface crack formation (IMC–B testing) is effective in investigating critical temperature ranges in the continuous casting process. The test series with Nb-microalloyed steel shows promising results and excellent reproducibility. It reveals the susceptibility to surface cracking during unbending in a slab caster depending on the Nb content and the prevalent surface temperature.

REFERENCES

1. J.K. Brimacombe and K. Sorimachi, “Crack formation in the continuous casting of steel”, *Metallurgical Transactions B*, Vol. 8, No. 3, 1977, pp 489.
2. B. Mintz, S. Yue and J.J. Jonas, “Hot ductility of steels and its relationship to the problem of transverse cracking during continuous casting”, *International Materials Reviews*, Vol. 36, No. 5, 1991, pp 187.
3. B. Mintz, “The influence of composition on the hot ductility of steels and to the problem of transverse cracking”, *ISIJ International*, Vol. 39, No. 9, 1999, pp 833.
4. R. Dippenaar, S.-C. Moon and E.S. Szekeres, “Strand surface cracks – The role of Abnormally-Large Prior-Austenite Grains”, *Proceedings AISTech*, 2006, pp 833.

5. E.S. Szekeres, “Overview of mould oscillation in continuous casting”, *Iron and Steel Engineering*, Vol. 73, No. 7, 1996, pp 29.
6. K. Schwerdtfeger, “Rißanfälligkeit von Stählen beim Stranggießen und Warmumformen”, Verlag Stahleisen mbH, Düsseldorf, Germany, 1994.
7. K. Schwerdtfeger and K.-H. Spitzer, “Application of Reduction of Area–Temperature Diagrams to the Prediction of Surface Crack Formation in Continuous Casting of Steel”, *ISIJ International*, Vol. 49, No. 4, 2009, pp 512.
8. C. Bernhard, P. Krajewski, T. Schaden und S. Ilie, “In-situ-Biegeversuch zur experimentellen Simulation der Bildung von Oberflächenrissen im Stranggießprozess“, *Fachausschuss für physikalische Chemie und metallurgische Verfahrensentwicklung des VDEh*, Düsseldorf, Germany, 2014.
9. B. Mintz, R. Abushosha and M. Shaker, “Influence of deformation inducted ferrite, grain boundary sliding and dynamic recrystallization on hot ductility of 0.1-0.75 %C steels”, *Material Science and Technology*, Vol. 9, 1993, pp 907.
10. B. Mintz, J. Lewis and J.J. Jonas., “Importance of deformation inducted ferrite and factors which control its formation”, *Materials Science and Technology*, Vol. 13, 1997, pp 379.
11. D.N. Crowther., “The Effects of Microalloying Elements on Cracking During Continuous Casting”, *The Use of Vanadium in Steel - Proceedings of the Vanitec Symposium*, Beijing, China, 2001, pp 99.
12. H. Presslinger, M. Mayr, E. Tragl and C. Bernhard, “Assessment of the Primary Structure of Slabs and the Influence on Hot- and Cold-Rolled Strip Structure”, *Steel Research Int.*, Vol. 77, No. 2, 2006, pp 107.
13. S. Ilie, J. Reiter, J. Fluch, H. Presslinger, and C. Bernhard, “Characterization of hot tear segregations in continuous casting of slabs”, *6th European Continuous Casting Conference*, Riccione, Italy, 2008, pp 122.
14. D.N. Crowther and B. Mintz, “Influence of grain size on hot ductility of plain C-Mn steels”, *Materials Science and Technology*, Vol. 2, 1986, pp 951.
15. D.N. Crowther and B. Mintz, “Influence of grain size and precipitation on hot ductility of microalloyed steels”, *Materials Science and Technology*, Vol. 2, 1986, pp 1099.
16. J.Y. Fu., C.I. Garcia, S. Pytel and A.J. DeArdo, “Hot ductility of continuously cast microalloyed steels”, *Processing, Microstructure and Properties of HSLA Steels*, 1988, pp 27.
17. J. Reiter, C. Bernhard and H. Presslinger, “Austenite grain size in the continuous casting process: Metallographic methods and evaluation”, *Materials Characterization*, Vol. 59, 2008, pp 737.
18. B. Mintz, “Importance of columnar grains in dictating hot ductility of steels”, *Materials Science and Technology*, Vol. 16, 2001, pp 1.
19. P. Krajewski, R. Krobath, C. Bernhard, J. Miettinen, S. Louhenkilpi, S. Ilie and T. Schaden, “A Novel Approach for the Simulation of Surface Crack Formation in Continuous Casting”, *BHM*, Vol. 160, No. 3, 2015, pp 109.
20. T. Revaux, P. Deprez, J.-P. Bricout and J. Oudin, “In Situ Solidified Tensile Test and Hot Ductility of Some Plain Carbon Steels and Microalloyed Steels”, *ISIJ International*, Vol. 34, No. 6, 1994, pp 528.
21. A.K. Guimelli, M. Militzer and E.B. Hawbolt, “Analyses of the Austenite Grain Size Distribution in Plain Carbon Steels”, *ISIJ International*, Vol. 39, No. 3, 1999, pp 271.
22. N. Fuchs, “In-situ Beobachtung von Austenitkornwachstum und Phasenumwandlungen in Stählen mittels Hochtemperatur-Laser-Scanning-Konfokal-Mikroskopie”, Master Thesis, Leoben, Austria, 2016.
23. C. Ouchi and K. Matsumoto, “Hot ductility in Nb-bearing high- strength steel low-alloy steels”, *Transactions ISIJ*, Vol. 22, 1982, pp 181.
24. N. Fuchs, P. Krajewski and C. Bernhard, “In-situ Observation of Austenite Grain Growth in Plain Carbon Steels by Means of High-temperature Laser Scanning Confocal Microscopy”, *BHM*, Vol. 160, No. 5, 2015, pp 214.